EFFECT OF PRE-AGEING ON NATURAL SECONDARY AGEING AND PAINT BAKE HARDENING IN AL-MG-SI ALLOYS

Zi Yang[1], Zeqin Liang[2], David Leyvraz[2], John Banhart[1]

[1]Helmholtz Centre Berlin, Hahn-Meitner-Platz, 14109 Berlin, Germany

[2]Novelis R&T Centre, Sierre, Rte des Laminoirs 15, 3960 Sierre, Switzerland

Supplementary material

A. Double ramping method for DSC

Conventional DSC baseline correction uses signals obtained in a baseline run with either empty crucibles or pure aluminium samples on both DSC stages before or after the actual measurement while applying the same DSC parameters. The disadvantage of this approach is that the samples for the measurement run are not the same as for the baseline run and the environment is also slightly changed during sample exchange. This often introduces a vertical offset as well as baseline drift on the DSC traces. This is critical for precipitation processes since the heat effect is generally small. In order to improve the baseline correction, we applied the double-ramping method which does not require sample exchanges during measurement [1]. An example of DSC traces obtained for sample PA *120/60* during both ramps is presented in Fig. S1. The subtraction of the second ramp (baseline) from the first ramp is the final curve used in Fig. 5c. In Fig. S1, the curves in the low- temperature regime (<100 °C) where no pronounced reactions are expected to occur are almost identical showing that the offset and baseline drift are indeed small. The disadvantage of this method is that the sample during the second ramp is only stable (no pronounced reactions) at relatively low temperatures. At higher temperatures, the baseline cannot be used due to pronounced reactions which drives the curve downwards (Fig. S1). However, this happens generally above ~320 °C, which is beyond the relevant precipitation peaks we study.
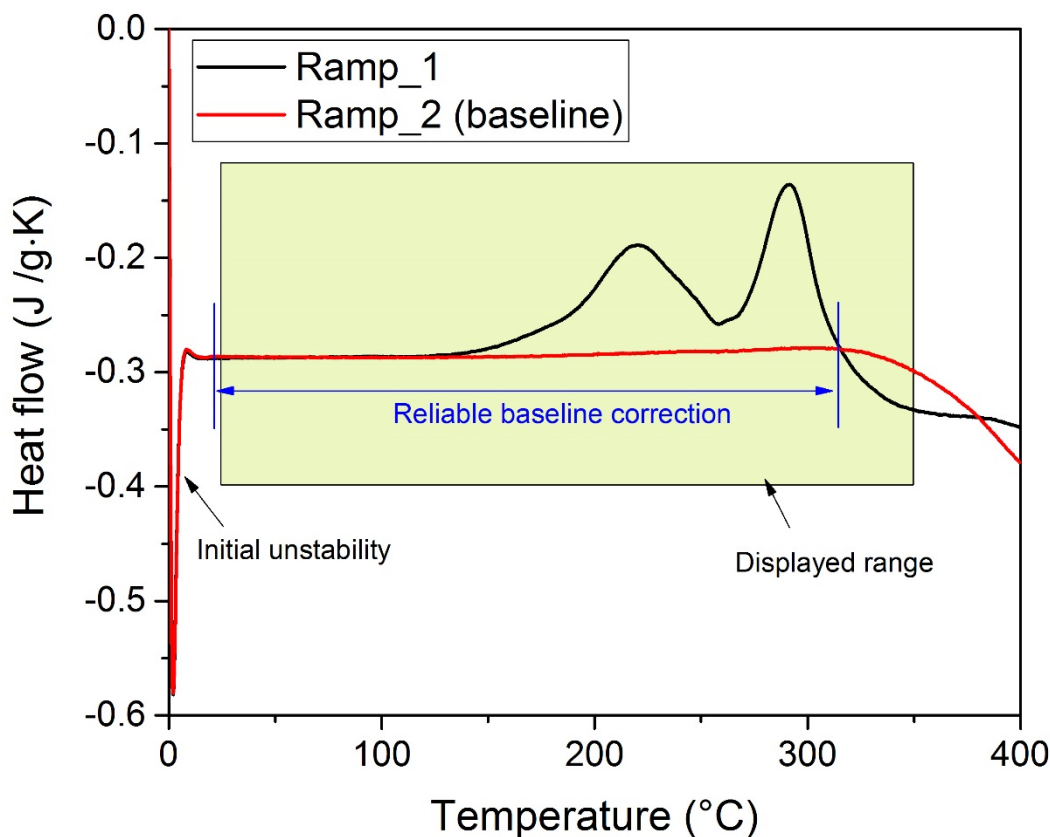
Fig. S1. Presentation of DSC traces obtained of a pre-aged sample (PA *120/60*) using the double-ramping method.

B. Positron lifetime measurements

PALS was conducted on a fast-fast coincidence spectrometer utilizing a 30 μCi ^{22}NaCO$_3$ positron source. The source and two samples (each $10\times10\times1$ mm^3) are packed in a "sandwich" geometry during measurement. The count rate of the spectrometer was ~950 s^{-1} and resolution (FWHM) ~0.254 ns. Single-component lifetimes were determined using software LT9 [2].

One-component positron lifetimes of an AQ sample and PA samples during NA/NSA are given in Fig. S2. For the AQ specimen, the initial positron lifetime τ_{1c} measured after 7 min of NA starts from ~233 ps and drops markedly to a minimum of ~222 ps within the first 120 min of NA. In the following, the lifetime rises up to a maximum ~225 ps and finally decreases to ~221 ps

2

after 1 week of NA. After PA, τ_{1c} starts from much lower values, namely ~219, ~217, and ~215 ps for PA *80/480*, PA *120/60*, and PA *160/10*, respectively. During NSA, τ_{1c} for PA *80/480* barely increases for up to 7000 min of NA, while for PA *160/10* and PA *120/60* a slight increase of τ_{1c} to ~220 ns can be observed. The onset of the lifetime increase is estimated by the extrapolation of the constant stage and increasing stage. It appears to start slightly earlier for PA *160/10* than for PA *120/60*.

τ_{1c} in the PALS signal after PA drops to 215 – 220 ps, which is the typical lifetime of positrons in clusters. The lower value for PA at higher temperature might result from ordering effects or a small bulk contribution due to a lower cluster density. During NSA τ_{1c} is stable for some time and then increases in analogy to NSA after cluster reversion (RA) [3]. Such an increase of lifetime is either caused by the increase of a component with higher lifetime or by reduction of a low-lifetime component [4-6]. The rise of a vacancy-related component is unlikely as well as a Mg enrichment of clusters because after PA at 80 °C the matrix should contain more Mg (and the clusters less) than after PA at 160 °C and therefore additional clustering is thought to increase the one-component (average) positron lifetime because the contribution of bulk annihilation (typical contribution ≤ 160 ps) is reduced.
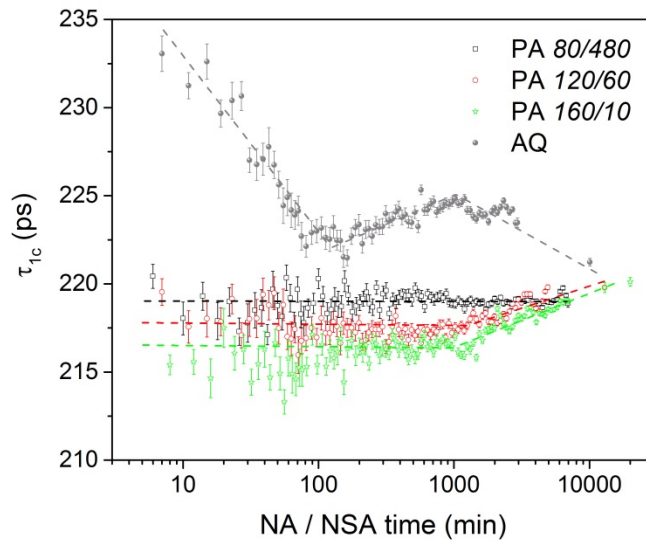
Fig. S2. Single-component positron lifetimes in AQ sample during NA or PA samples (similar hardness ~60 HBW) during NSA. Dashed lines are guidelines.

C. Additional DSC data

Fig. S3a – c shows DSC traces of alloys pre-aged at 100 °C for 60 min, 240 min, and pre-aged at 120 °C for 60 min and then NSA for various times. The trends of the DSC curve evolution for increasing NSA time is similar, just that the influence of the same NSA time on the DSC curve depends on the PA condition. The heat content for clustering during ageing (PA and/or NSA) can be estimated by $\Delta H_\text{ageing} = H_\text{AQ} - H_\text{after ageing}$, where H is the integrated DSC heat flow from T_a to T_e, $H = \int_{T_a}^{T_e} \frac{dQ}{dt} dT$. T_a is the temperature before the first reaction begins, and T_e the temperature at which equilibrium is reached, e.g. above the solution heat treatment temperature. However, as pointed out by Esmaeili et al. [7, 8], due to a high baseline drift in the higher temperature regime, a lower T_e can also be chosen as long as all relevant precipitation/dissolution peaks are covered within the temperature range. We choose $T_a = 50$ °C and $T_e = 315$ °C because DSC curves before T_a and after T_e are converged. H_AQ is constant, thus $H_\text{after ageing} = \Delta H_\text{ageing} + H_\text{AQ}$. Fig. S3d shows hardness plotted as a function of the DSC integral for samples pre-aged and subsequently naturally aged (in cases where DSC and hardness were both measured). A linear relationship is seen although with some fluctuations possibly due to different samples and possibly some baseline drift. If the heat signal is assumed to be proportional to the precipitated volume the latter is also proportional to hardness after NSA.
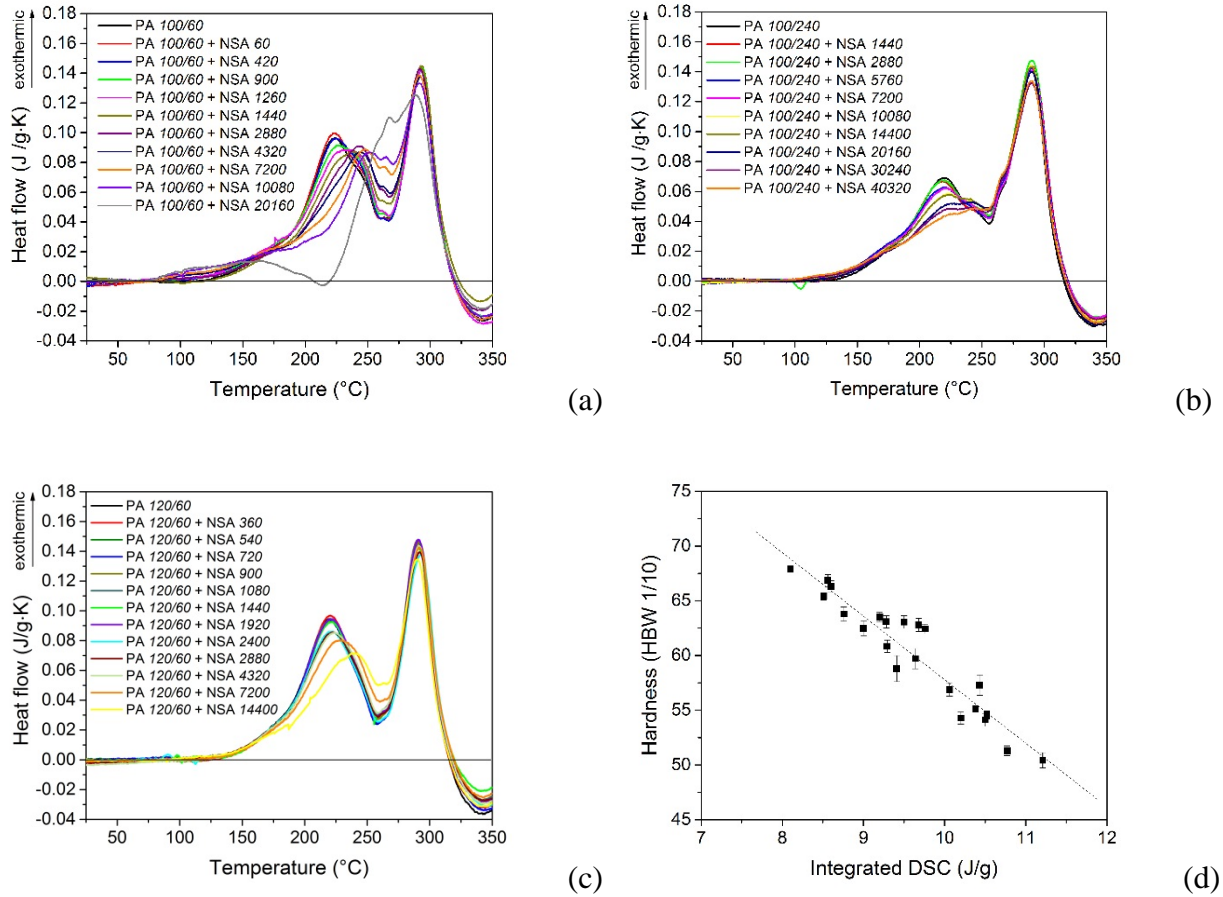
Fig. S3. DSC traces of samples PA a) at 100 °C for 60 min, (b) 240 min, (c) PA at 120 °C for 60 min with and without ensuing NSA. (d) Hardness as a function of integrated DSC heat flow from 50 °C to 315 °C using hardness data presented in Fig. 3a,c and DSC data in Fig. 5d and Fig. S3a – c (whenever both hardness and DSC are measured for the same NSA time).

D. Possible other cluster strengthening mechanism

PA clusters formed at different temperatures but yielding the same hardness were assumed in Sec. 4.2.2 to consume the same fraction of solute supersaturation. Now we discuss if clusters formed at different temperatures have a different strengthening effect. The 'Weak obstacle' model [10-12] assumes a relationship between hardness increase and fraction of solute clusters, $\Delta \mathcal{H} \propto \sqrt{\alpha} \cdot$

$\sqrt{r}$ with r the radius of solute clusters. Since clusters formed at higher temperature have a larger radius on average [13], a smaller fraction of solutes is consumed when the same hardness is reached by PA at higher temperature. As a consequence, the retardation factor ratio will be smaller than the one following from Fig. 8 if the same solute fraction has to be consumed at different PA temperatures. This does not affect the main conclusions of the work.

(a)   (b)
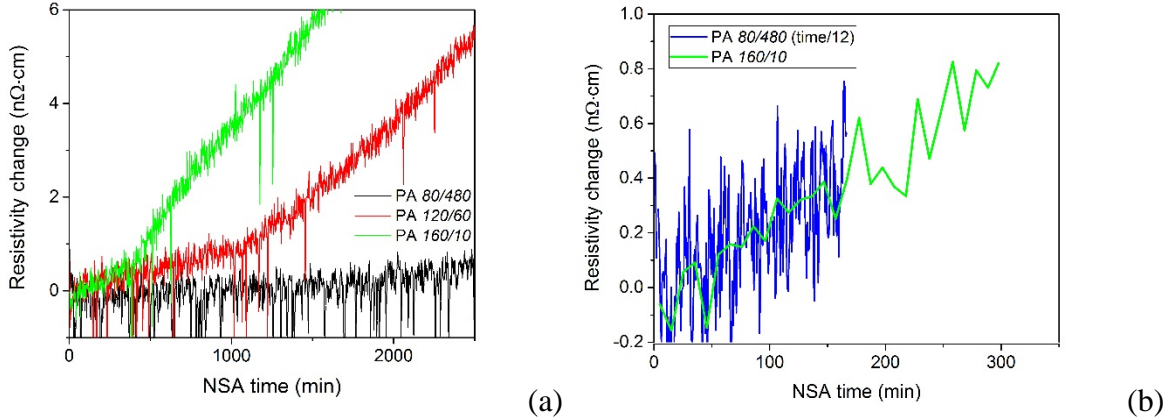
Fig. S4. (a) Same as Fig. 4d but plotted with linear NSA time. (b) the initial linear increase stage of PA *80/480* and PA *160/10*. Curves in (b) have been smoothed by filtering artefact data points (sudden drops [9]) and averaging every 5 points.

E.   Retardation factor from resistivity measurements

Retardation factors were determined using hardness curves and collapsing them into one master curve by normalising the NSA time with Θ^{-1}. As electrical resistivity is more sensitive to clustering than hardness, it might detect earlier changes during NSA. Fig. S4 shows the data of Fig. 4d on a linear time scale. A linear increase is found at the beginning of NSA with almost no incubation time. Thus the retardation factor can be calculated from the slope of the initial resistivity increase [3]. Here relative retardation of PA *80/480* to PA *160/10* is 12, which is larger than the value obtained from hardness ($\mathcal{R}_\theta \approx 3$) but still smaller than the ratio between PA equilibrium vacancy concentrations ($\mathcal{R}_c \approx 58$). This underlines the importance of PA clusters in determining the mobile vacancy concentration and strengthens the arguments in Sec. 4.2.2. The main conclusions remain the same.

F. Modelling of NSA clustering

In the main text of the present paper, we showed that NSA hardening is delayed after applying PA, and especially, to different extents when PA temperature varies while keeping PA hardness constant (as long as >55 HBW). NSA kinetics is faster after PA at higher temperature (for a shorter time) than at lower temperature (for a longer time), with a factor of ~3 for PA at 160 °C and 80 °C, whereas the equilibrium mobile vacancy concentration at 160 °C is ~58 times higher than at 80 °C.

Here we discuss whether such discrepancy can be explained by vacancy losses due to annihilation at sinks or vacancy trapping in NSA clusters (Zurob's model [14]). The kinetic master equation (Eq. (1) in the main text) is simplified here to Eq. (S1) using α_{NSA} to represent the relative fraction of total clustered solutes during NSA, and $(1 - \alpha_{NSA})$ as the simple function related to supersaturation i.e. $\varphi \equiv 1$. Since we have a non-equilibrium excess vacancy concentration, which is influenced concurrently by annihilation kinetics and trapping, we solve the master equation numerically instead of analytically.

$$\frac{d\alpha_{NSA}}{dt} = a \times (1 - \alpha_{NSA}) \times c_{\text{vac}}(t), \quad \text{with } a \text{ a constant.} \tag{S1}$$

F1. Vacancy annihilation during NSA

Two excess vacancy annihilation models were found in the literature, proposed by Schulze et al.[15, 16] and Fischer et al. [17] respectively. Schulze's model assumes that the annihilation rate of vacancies is proportional to the excess vacancy concentration to a power of q (Eq. (S2), where $q = 1$ is the most simple case [15]), while Fischer's model gives an annihilation rate in Eq. (S3) if we consider only annihilation at dislocation jogs and no hydrostatic stress. b_1, b_2 are both constants governing kinetics. For both models, the difference between the vacancy concentrations after PA at 160 °C and 80 °C starts with ~58 at the beginning of NSA and gradually goes to 1 during NSA, as illustrated in Fig. S5. The difference between the two models is Fischer's model eliminates the vacancy discrepancy faster than Schulze's model ($q = 1$). Thus, Fischer's model will be used in the following discussion.

$$\frac{dc_{\text{vac}}(t)}{dt} = b_1 \times \left(c_{\text{vac}}(t) - c_{\text{vac}}^{\text{eq}}\right)^q \tag{S2}$$

$$\frac{dc_{\text{vac}}(t)}{dt} = b_2 \times c_{\text{vac}}(t) \times \ln\left(\frac{c_{\text{vac}}(t)}{c_{\text{vac}}^{\text{eq}}}\right) \tag{S3}$$

7

(a)   (b)
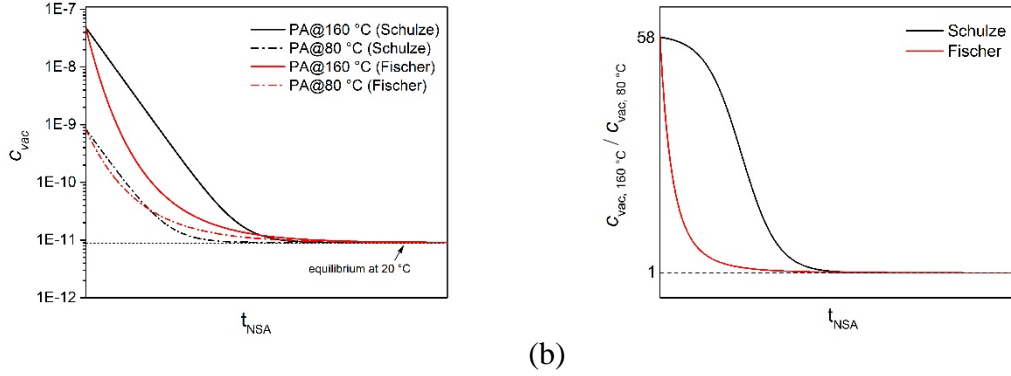
Fig. S5. (a) Schematic evolution of vacancy fraction during NSA after PA at different temperatures. b_1 and b_2 are adjusted to produce similar annihilation kinetics after PA at 80 °C by both models. Fischer's model gives much faster annihilation after PA at 160 °C. (b) Ratio of the vacancy concentrations during NSA after PA at different temperatures.

F2. Vacancy trapping by NSA clusters

Here we take into account that vacancies are trapped by emerging NSA clusters. One model describing such phenomenon was established by Zurob et al. [14] by assuming that the probability of a trapped vacancy to escape from a cluster is proportional to the Boltzmann weight of the interaction energy between the cluster and the vacancy, which is proportional to the number of solute atoms in the cluster due to the number of successful jumps required to escape from the cluster. If the number of clusters remains constant and just their size increases during NSA, then we can express the mobile vacancy concentration by Eq. (S4), where m and n are adjustable constants, and n is negative. Note that this model is based on kinetic arguments, which is different from the thermodynamic approach proposed by Pogatscher et al. [18], although they result in similar equations. Since only mobile vacancies can annihilate, $c_{\mathrm{vac}}(t)$ in Eq. (S3) has to be replaced by $c_{\mathrm{vac,mob}}(t)$ when vacancy trapping is considered.

$$\frac{c_{\mathrm{vac,mob}}(t)}{c_{\mathrm{vac}}(t)} = m \times \exp(n \times \alpha_{NSA}). \tag{S4}$$

Using the above mentioned models, i.e. Eq. (S3) and (S4) with $c_{\mathrm{vac}}(t)$ in Eq. (S3) replaced by $c_{\mathrm{vac,mob}}(t)$, Fig. S6 demonstrates the simulated kinetics during NSA after PA at two representative temperatures (160 °C and 80 °C) under various vacancy annihilation and trapping effects by changing the adjustable constant parameters. The initial kinetic difference stems from

different equilibrium vacancy concentrations at 160 °C and 80 °C (factor 58). This difference remains (weak annihilation or strong trapping) or gets larger, but is not reduced to 3 as obtained from the experiments.
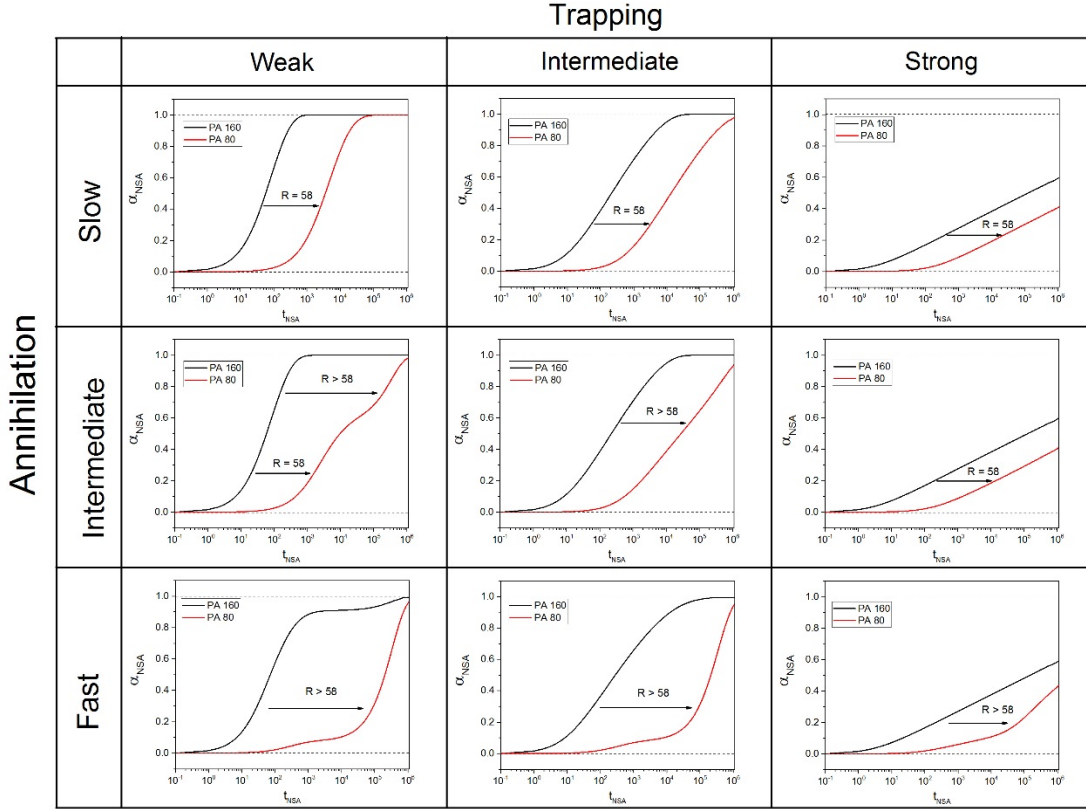
Fig. S6. Schematic representation of α_{NSA} as a function of t_{NSA} after PA at 160 °C and 80 °C under various vacancy annihilation and trapping conditions. Stronger trapping: n decreases (more negative). Faster annihilation: b_2 increases.

G. Vacancy trapping by PA clusters.

During PA, it is assumed that the equilibrium vacancy concentration is reached. Taking into account vacancy trapping by PA clusters, the total vacancy fraction is higher than at thermal equilibrium. The fraction η of mobile vacancies with respect to the total vacancy fraction depends on the interaction energy, number of trapping sites, and temperature as vacancy jump are thermally activated. Fig. S7 shows η as a function of temperature calculated by Eq. (4) based on estimated values of the interaction energy and trapping site number. The thermal vacancy site fractions at 160 °C and 80 °C have a ratio of 58. However, the stronger trapping effect at 80 °C

reduces the ratio of total vacancies to < 58 and NSA kinetics become more similar at the two temperatures.
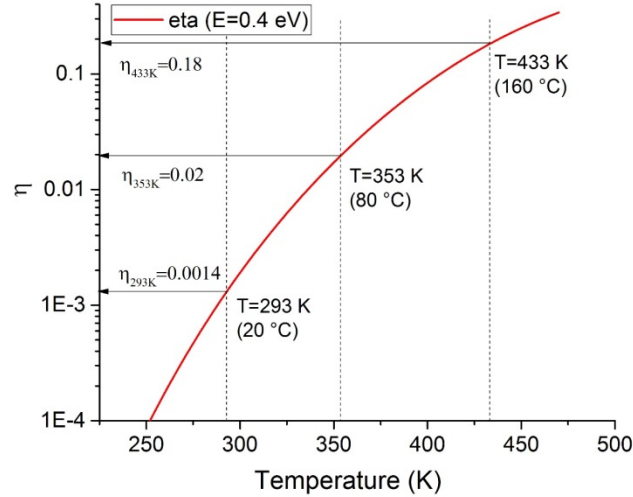
Fig. S7. Fraction of mobile vacancies η as a function of temperature calculated using Eq. (4) and an interaction energy of $E = 0.4$ eV and trapping site fraction $x_{ts} = 10^{-4}$. The former is estimated to be comparable to Sn-Vacancy binding, while the latter derives from a typical cluster site fraction. These numbers have been chosen to illustrate the trapping effect qualitatively and do not originate from precise calculations.

Zurob et al. [14] proposed that the interaction energy between vacancies and clusters scales with the size of clusters, i.e., the trapping energy is higher for larger clusters. Thus, if the interaction energy E_1 for clusters formed at 160 °C is higher than E_2, for clusters formed at 80 °C, and the total number of trapping sites x_{ts} is constant, the ratio between mobile vacancy concentrations at NSA temperature encountered after PA at these two temperatures is given by

$$\mathcal{R}_c = \frac{c_{vac,160}^{eq}}{c_{vac,80}^{eq}} \times \frac{1 + x_{ts}\exp\left(\frac{E_1}{kT_{160}}\right)}{1 + x_{ts}\exp\left(\frac{E_2}{kT_{80}}\right)} \times \frac{1 + x_{ts}\exp\left(\frac{E_2}{kT_{20}}\right)}{1 + x_{ts}\exp\left(\frac{E_1}{kT_{20}}\right)}. \tag{S5}$$

It is not hard to calculate that $\mathcal{R}_c < 58$ is still valid if $E_1 > E_2$.

References

[1] A. Deschamps, M. Garcia, J. Chevy, B. Davo, F. De Geuser, Influence of Mg and Li content on the microstructure evolution of Al-Cu-Li alloys during long-term ageing, Acta Materialia 122 (2017) 32-46.

[2] J. Kansy, Microcomputer program for analysis of positron annihilation lifetime spectra, Nuclear Instruments and Methods in Physics Research A 374 (1996) 235-244.

[3] M. Madanat, M. Liu, J. Banhart, Reversion of natural ageing in Al-Mg-Si alloys, Acta Materialia 159 (2018) 163-172.

[4] J. Banhart, M.D.H. Lay, C.S.T. Chang, A.J. Hill, Kinetics of natural aging in Al-Mg-Si alloys studied by positron annihilation lifetime spectroscopy, Physical Review B 83(1) (2011) 014101.

[5] M. Liu, Clustering kinetics in Al-Mg-Si alloys investigated by positron annihilation techniques, Technische Universität Berlin, Berlin, 2014.

[6] M. Liu, J. Cizek, C.S.T. Chang, J. Banhart, Early stages of solute clustering in an Al–Mg–Si alloy, Acta Materialia 91 (2015) 355–364.

[7] S. Esmaeili, X. Wang, D.J. Lloyd, W.J. Poole, On the precipitation-hardening behavior of the Al-Mg-Si-Cu, Metallurgical and Materials Transactions A 34A(3) (2003) 751-763.

[8] S. Esmaeili, D.J. Lloyd, Characterization of the evolution of the volume fraction of precipitates in aged AlMgSiCu alloys using DSC technique, Materials Characterization 55(4-5) (2005) 307-319.

[9] M. Wüstenhagen, Entwicklung des elektrischen Widerstandes von Al-Mg, Al-Si und Al-Mg-Si Legierungen während der Kaltauslagerung, Thesis, TU Berlin (2016).

[10] S. Esmaeili, D.J. Lloyd, W.J. Poole, Modeling of precipitation hardening for the naturally aged Al-Mg-Si-Cu alloy AA6111, Acta Materialia 51(12) (2003) 3467-3481.

[11] S. Esmaeili, D.J. Lloyd, W.J. Poole, A yield strength model for the Al-Mg-Si-Cu alloy AA6111, Acta Materialia 51(8) (2003) 2243-2257.

[12] R.K.W. Marceau, A. de Vaucorbeil, G. Sha, S.P. Ringer, W.J. Poole, Analysis of strengthening in AA6111 during the early stages of aging: Atom probe tomography and yield stress modelling, Acta Materialia 61(19) (2013) 7285-7303.

[13] M.W. Zandbergen, Q. Xu, A. Cerezo, G.D.W. Smith, Study of precipitation in Al-Mg-Si alloys by atom probe tomography I. Microstructural changes as a function of ageing temperature, Acta Materialia 101 (2015) 136-148.

[14] H.S. Zurob, H. Seyedrezai, A model for the growth of solute clusters based on vacancy trapping, Scripta Materialia 61(2) (2009) 141-144.

[15] H.A. Schulze, K. Lücke, Short-Range-Order Formation in Dilute Alloys due to Quenched-in Vacancies, Journal of Applied Physics 39 (1968) 4860-4862.

[16] H.A. Schulze, K. Lücke, The influence of vacancies on short-range order formation in Au-Ag alloys, Acta Metallurgica 20 (1972) 529-542.

[17] F.D. Fischer, J. Svoboda, F. Appel, E. Kozeschnik, Modeling of excess vacancy annihilation at different types of sinks, Acta Materialia 59 (2011) 3463-3472.

[18] S. Pogatscher, H. Antrekowitsch, M. Werinos, F. Moszner, S.S.A. Gerstl, M.F. Francis, W.A. Curtin, J.F. Löffler, P.G. Uggowitzer, Diffusion on Demand to Control Precipitation Aging: Application to Al-Mg-Si Alloys, Physical Review Letters 112 (2014) 225701.